Mapping thermal resistance around vacancy defects in graphite

Laura de Sousa Oliveira and P. Alex Greaney
School of Mechanical, Industrial, & Manufacturing Engineering
Oregon State University, Corvallis, OR 97331

ABSTRACT

High purity bulk graphite is applicable in many capacities in the nuclear industry. The thermal conductivity of graphite has been found to vary as a function of how its morphology changes on the nanoscale, and the type and number of defects present. We compute thermal conductivities at the nanolevel using large scale classical molecular dynamics simulations and by employing the Green-Kubo method in a set of *in silico* experiments geared towards understanding the impact of defects in the thermal conductivity of graphite. We present the results obtained for systems with 1–3 vacancies, and compile a summary of some of the methods applied and difficulties encountered.

INTRODUCTION

Graphite is applicable in many capacities in the nuclear industry. It is used in gaskets, sealants, and liners, but most importantly, it is used as a moderator and a reflector, and its unique properties are being exploited in order to develop high-tech fuel elements for next-generation nuclear reactors. While graphite has been comprehensively studied since the 1950s [4], there are aspects of its thermal conductivity (κ) which have yet to be well understood. Graphite is highly anisotropic and the thermal conductivity along the basal plane (κ_a) differs significantly from that along the c-axis (κ_c), with an experimentally computed anisotropy ratio (κ_a/κ_c) just below 210 at 300K in near-ideal graphite [3]. Furthermore, the thermal conductivity in bulk graphite varies as a function of how the material is manufactured and its exposure to radiation and high temperatures within a reactor. Our motivation is to establish a systematic understanding of how defect type, number and different defect-type ensembles affect thermal resistance in graphite. Defects can occur at different scales, and while grain boundaries, porosity and amorphous regions, for instance, can significantly affect thermal transport, in our first steps towards achieving our goal we examine point defects. In this Proceedings paper we report on a collection of vacancy defects. In addition, we summarize the methods we have developed for studying phonon scattering around defects and some of the difficulties that arise when computing κ in graphite.

METHODS

Simulations were performed using large-scale equilibrium classical molecular dynamics. More specifically, we use the LAMMPS [6] software, distributed by Sandia National Laboratories. Molecular dynamics (MD) is a powerful tool for understanding thermal behavior and phonon scattering. However, there are several limitations to MD that make qualitative predictions of thermal conductivity unlikely. To mitigate this and to gain insight into how thermal resistance varies at the atomic-level and as a function of the different defects, we perform a comparative analysis. In this study, we compare the thermal conductivity and corresponding anisotropy ratios obtained between the different defective systems and the perfect crystal, as well as in different regions within each system. κ is computed along each axis, for each system and in specific regions within each system,

by employing the AIREBO [7] [1] potential, as it is implemented in the LAMMPS MD package, and the Green-Kubo formulation [2] [5] in the microcanonical ensemble (NVE). The Green-Kubo method (see Equation 1), derived from the fluctuation-dissipation theorem, utilizes the ensemble average of the autocorrelation of the instantaneous heat flux (J) to compute κ in a given direction. In Equation 1, T is the temperature in the system or region considered, V is the corresponding volume, and k_B is Boltzmann's constant.

$$\kappa_x = \frac{V}{k_B T^2} \int_0^\infty \left\langle J_x(t) J_x(t+\Delta t) \right\rangle \, dt \tag{1}$$

To map the local thermal conductivity we divide the compute cell into a system of 550 overlapping sub-regions (5, 10, and 11 along the x, y and z directions respectively). J is computed in each sub-region, and its autocorrelation function integrated to produce a local κ. The regional κ values obtained are used to compute iso-surface maps, which are discussed in the Results section. The perfect crystalline system simulated consists of 10648 atoms, approximately $(265.6 \times 459.6 \times 758.2)$ nm^3, from which 1–3 atoms are removed along the basal plane, in a centrally located region of the system (see Fig. 1). The difference in the size of the system along the x and y directions results in different thermal conductivities along these axes and allows us to identify size artifacts.

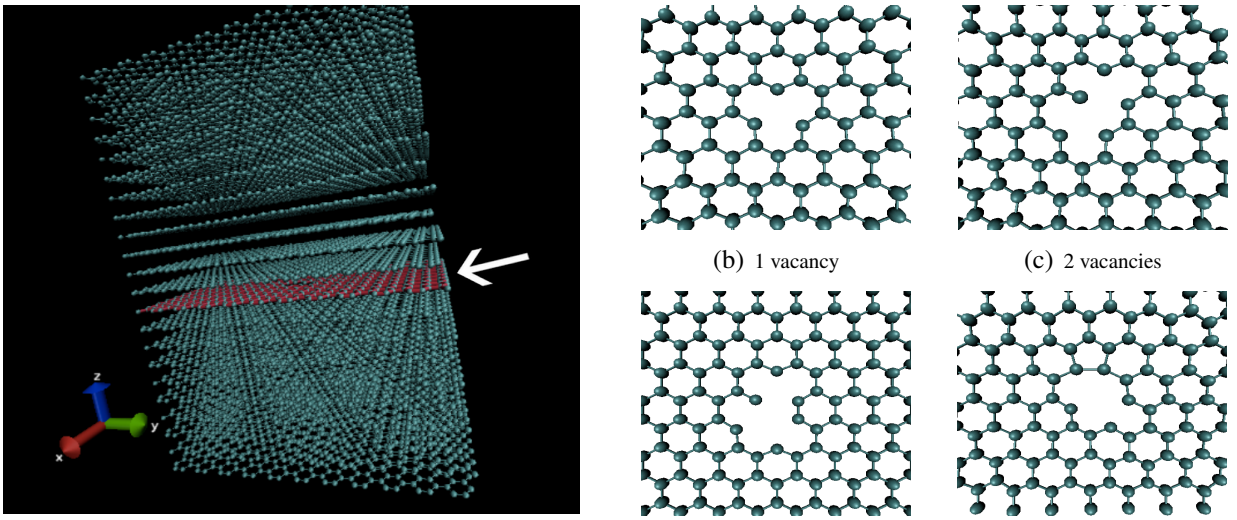

(a) Location of the vacancies within the system.

(b) 1 vacancy

(c) 2 vacancies

(d) 3 vacancies — initial set up

(e) 3 vacancies — during simulation

Figure 1: In (a), the arrow points to where both the single vacancy and the 2–3 in-plane vacancy clusters are placed within each system. This image corresponds to the cluster with 3 vacancies. (b) and (c) illustrate the single vacancy and double vacancy cluster within the plane, respectively. (d) shows where the three vacancies are originally introduced, and (e) shows how the atoms rearrange themselves during the NVT simulation.

The perfect and defective systems are simulated at 300 K* with a time step of 2×10^{-7} ns for a total duration of 0.6 ns. The autocorrelation is computed for 0.015 ns. The isothermal-isobaric ensemble (NPT) is used to bring the systems to 300 K, at which point we switch to NVE and

*It is important to note that while this is well below the Debye temperature, our goal is a comparative analysis of phonon scattering from and around the defect — not phonon-scattering.

simulate them for different lengths of time in order to obtain different initial atomic arrangements for each system. Overall, our results are averaged over 20 separate simulations for the perfect crystalline system, 11 simulations for the 2–vacancy-cluster, and 10 simulations for the remaining defective systems.

FEATURES OF THE AUTOCORRELATION FUNCTION

When computing the autocorrelation, it was observed that rare events take place which make a rapid and large change to the total heat current autocorrelation function $\left(\left\langle J_X(t)J_X(t+\Delta t)\right\rangle\right)$. These fluctuations require a long averaging time to diminish and are more prevalent in the heat current along the basal plane than along the c-axis. The rare events, examples of which can be seen in Figs. 2(a), (b) and (c) are not present in every run, but when they occur they are large enough to affect the resulting κ. To obtain a statistically significant sample of runs which would include them, we simulate multiple system sizes for the perfect crystalline graphite and, using the same method described in the Methods section, produce several runs for each system size. It is possible that these events are artifacts of the system size; however, we do not notice any reduction in the number of these events with increasing system size. Alternatively, the rare fluctuations observed could be a manifestation of the Fermi–Pasta–Ulam–Tsingou problem. The effect these rare fluctuations have on the thermal conductivity is best illustrated in Figs. 2(d), (e) and (f), which shows κ computed as a simulation progresses. In other words, for each autocorrelation plotted as in Figs. 2(a), (b) and (c) there is a corresponding κ value obtained with the Green-Kubo formulation by integrating along the "Autocorrelation Time" axis — these are plotted for many simulations in Figs. 2(d), (e) and (f). While it is clear that κ tends to converge, we can observe spikes in its value along some runs, which may occur at any time within a given run, even as it appears to be converging, and which lasts for varying periods of time. In response to these events, several protocols for computing thermal conductivities using different integrating schemes (see Fig. 3) were tested. Specifically, we truncated the autocorrelation function at different times, and tried integrating multiple exponential fits to the autocorrelation (only the best fit obtained is actually shown in Fig. 3). Integrating the autocorrelation for 15 ps yields systematically higher thermal conductivities, but larger error bars. Since the rare events do not take place in every run and affect each run differently, integrating over the tail of the autocorrelation function increases the variability of the resulting κ values, resulting in larger error bars. Integrating for a shorter amount of time will exclude the tail and result in consistently smaller values of κ, but does reduce the error bars. Ultimately we are constrained by computer time. Our goal is to gather as good statistics — including rare events — as possible that allow a meaningful comparison of predicted κ values that are not distorted by a low number of events. To this end, we are willing to underestimate kappa in return for performing more, shorter simulations to improve ergodic sampling. Provided that we adhere to the same integration protocol, we should be able to derive significant insight from the various defective systems simulations concerning how the thermal resistance in graphite is affected by point defects.

While LAMMPS may be used to compute the autocorrelation function for the entire system, to compute maps for how the thermal conductivities vary within each system, we use our own code to compute the autocorrelations. The code was test for agreement with LAMMPS, as can be seen in Fig. 3. The following results are computed using our code.

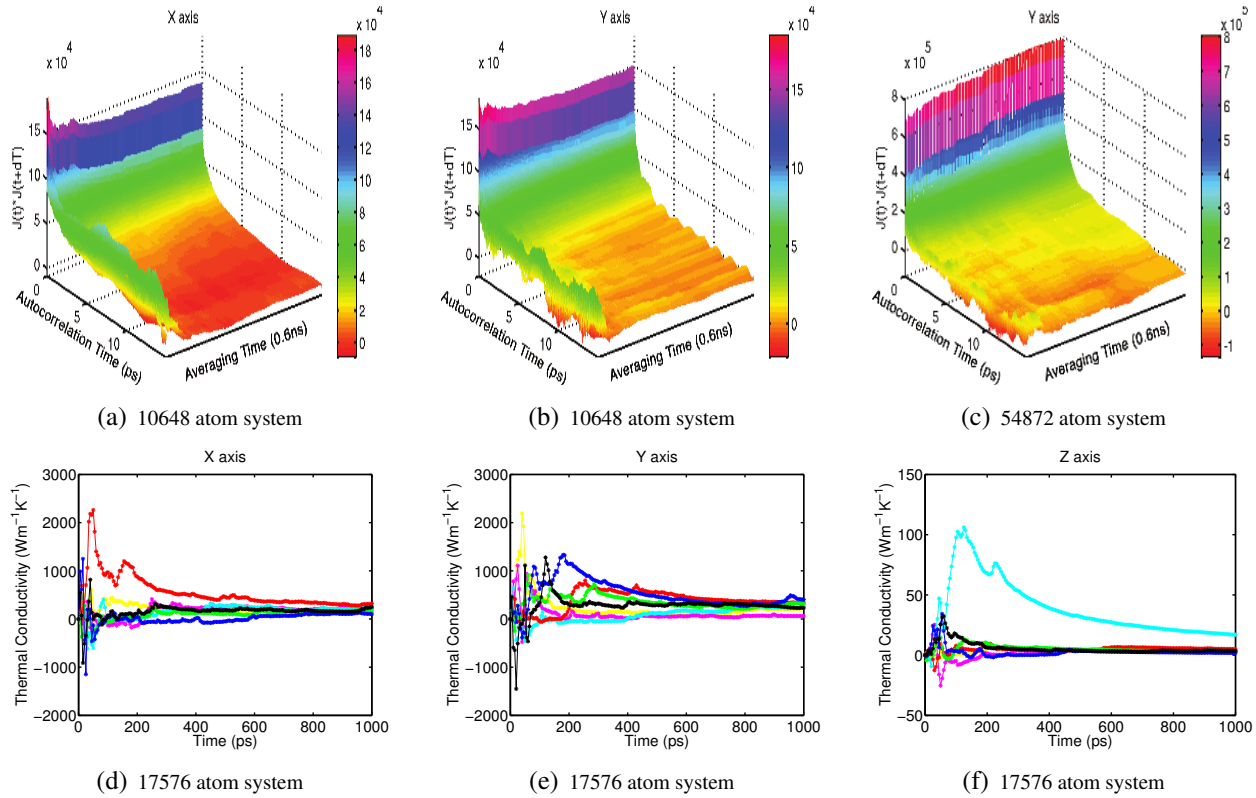

(a) 10648 atom system (b) 10648 atom system (c) 54872 atom system

(d) 17576 atom system (e) 17576 atom system (f) 17576 atom system

Figure 2: In the first horizontal block of figures, the autocorrelation has been plotted multiple times as it is computed (and thus averaged) as the simulation progresses. Initially, there are few values that contribute towards the ensemble average and thus the initial autocorrelation functions are noisy. As the averaging time progresses the autocorrelations become smoother with the exception of well-defined crests and troughs (aforementioned as rare events) which fade slowly, or not at all during the total simulation time. (a) and (b) correspond to the same run in x and y, respectively. (c) shows the autocorrelations of the instantaneous heat-flux computed over time in the x direction for a perfectly crystalline system with 54872 atoms. The second block of figures ((d)–(f)) corresponds to a 17576 atom system and each curve color corresponds to a a single run. Each plot corresponds to x, y and z values. The thermal conductivity values are obtained using the autocorrelation function computed at different run times for each run within each system.

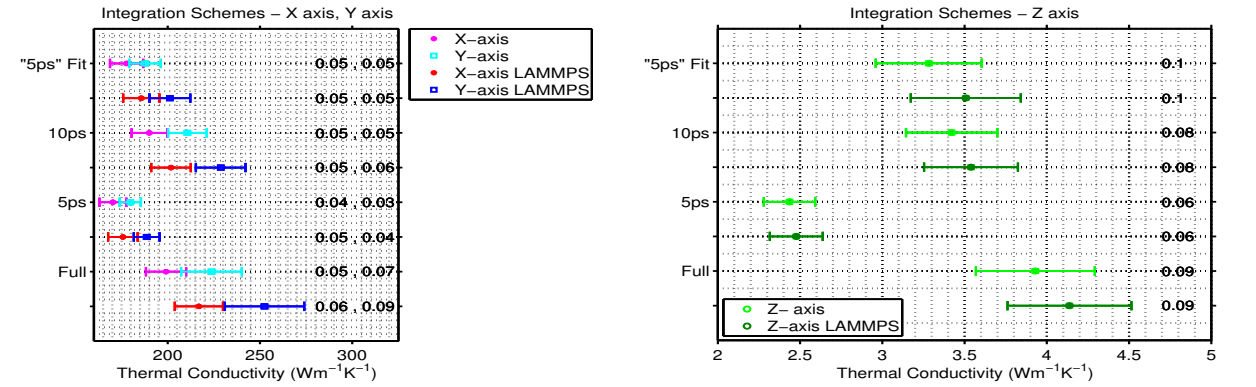

(a) Integration protocols - X, Y axis (b) Integration protocols - Z axis

Figure 3: While these plots correspond to the 10648 atom system, the change in the error bars and thermal conductivity values with respect to the integrating scheme is systematically the same for all systems. The numbers on the right of each plot correspond to the relative standard error (not normalized out of 100%) for the x and y-axis, respectively, in (a) and for the z-axis, in (b). The first values for each protocol correspond to the autocorrelation function computed with our code.)

RESULTS

The thermal conductivity values obtained in each axis for the different vacancy cluster defects and the perfect system can be found in Fig. 4. While there is no statistically significant change in

κ along the c-xis, we observe significant differences in the κ_x and κ_y values between the perfect system and the 2 and 3–vacancy-clusters. In these clusters we see the thermal conductivity go up with respect to the perfect crystal and the single-vacancy defect, and in the 3–vacancy-cluster case, we observe a large difference between κ_x and κ_y. During the simulations, the vacancy and the vacancy-clusters diffuse along the plane they were inserted in. The anisotropy ratios (Fig. 4(c)) reflect the combined changes in the thermal conductivities along the basal plane and along the c-axis.

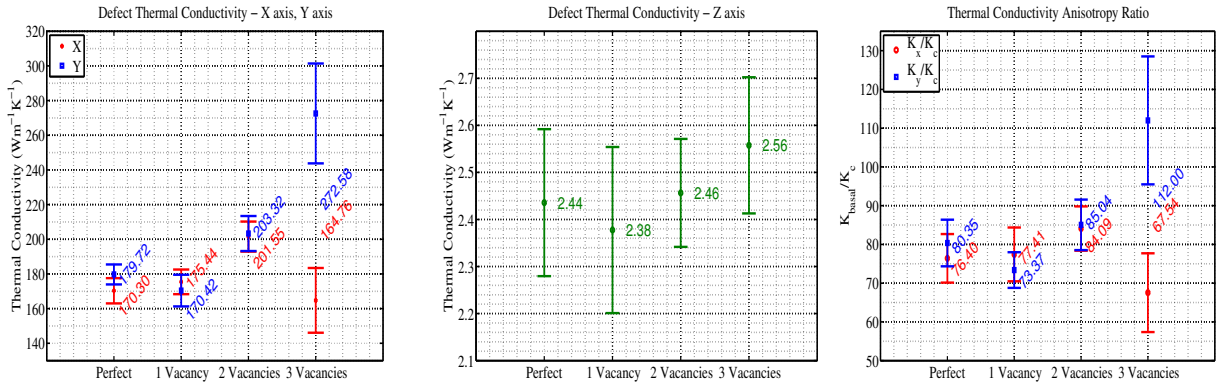

(a) κ along the basal plane (b) κ along the z-axis (c) κ anisotropy ratios

Figure 4: (a) and (b) are the κ values obtained for the perfect, the single-vacancy and 2 and 3–vacancy-cluster systems, both along the basal plane ((a)) and along the c-axis ((b)). (c) is the anisotropy ratio computed for both x and y.

The following κ-maps (Fig. 5) were intended to shed some light on how the thermal conductivities change around the defects. These maps were obtained by plotting the iso-surfaces of κ using regionally computed thermal conductivities, i.e., by integrating the local J correlation function. These maps are very noisy and show no systematic local change in κ. This could be possibly due to the diffusion of the vacancy and the vacancy-clusters. While it is interesting that the noise is stratified and that the fluctuations in thermal conductivity between regions are large, there doesn't seem to be a clear distinction between how thermal conductivities propagate and what their values are in the regions near the defects. Table 1 contains the ratios between the maximum and minimum thermal conductivity values found within each system, and there appears to be no significant difference between the maximum and minimum regional κs between systems.

	Perfect System	1 Vacancy	2 Vacancies	3 Vacancies
Max(κ_x)/Min(κ_x)	5.1987	7.18629	6.48254	9.09487
Max(κ_y)/Min(κ_y)	7.71476	9.85168	12.0638	13.6437
Max(κ_z)/Min(κ_z)	27.0945	24.7075	7.61275	10.6363

Table 1: Ratios between the maximum and minimum mean regional thermal conductivities within each system.

CONCLUSION

We have computed thermal conductivities of graphite containing a collection of vacancy defects. In doing so, we have found that the vacancy-clusters increase the thermal conductivity in-plane,

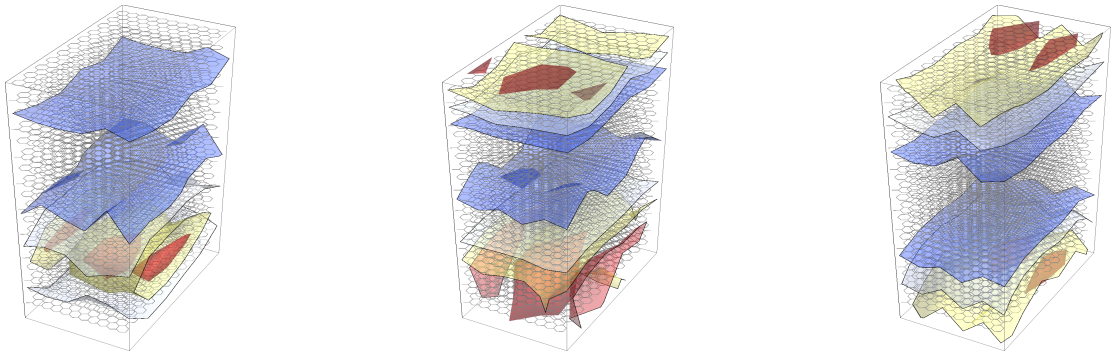

(a) Perfect - Y-axis (b) Perfect - Z-axis (c) 3 Vacancies - Y-axis

Figure 5: Thermal conductivity maps. (a) and (b) correspond to the y and z (in this order) thermal conductivity iso-surfaces obtained for a perfect system. (c) corresponds to the 3–vacancy-cluster, in the y direction. These maps were computed from the mean value of κ obtained for 550 regions for each system.

but not along the c direction – it is, thus, possible that this is due to tension in the plane caused by the presence of the clusters. In these simulations, we observe how large fluctuations in the heat current correlation function pose a challenge for the prediction of κ. Finally, we have mapped κ locally around defects. Thus far, these maps do not account for the cross correlation of energy current between regions, but will do so in the future as we continue to develop them.

ACKNOWLEDGMENTS

We thank Phillip Jenks and Rodrigo Lopes for their assistance with some of the C++ code. This work used the Extreme Science and Engineering Discovery Environment (XSEDE), which is supported by the National Science Foundation grant number OCI-1053575.

REFERENCES

[1] Harrison, Stuart, Ni, Sinnott, Brenner, Shenderova. *J. Phys: Cond. Matt.*, 14:783–802, 2002.

[2] Melville S. Green. time-dependent phenomena. ii. irreversible processes in fluids. *The Journal of Chemical Physics*, 22(3):398–413, 1954.

[3] CN Hooker, AR Ubbelohde, and DA Young. *Proceedings of the Royal Society of London. Series A. Mathematical and physical sciences*, 284(1396):17–31, 1965.

[4] B.T. Kelly. *Physics of Graphite*. RES mechanica monographs. Kluwer Academic Pub, 1981.

[5] Ryogo Kubo. theory and simple applications to magnetic and conduction problems. *Journal of the Physical Society of Japan*, 12(6):570–586, 1957.

[6] Steve Plimpton et al. *Journal of Computational Physics*, 117(1):1–19, 1995.

[7] Harrison Stuart, Tutein. *J. Chem. Phys*, 112:6472–6486, 2000.